Ore Geology Reviews 144 (2022) 104826

Contents lists available at ScienceDirect

Ore Geology Reviews

journal homepage: www.elsevier.com/locate/oregeorev

Breccia and vein mineralization of the Balatoc Diatreme, Acupan gold deposit, Baguio Mineral District: An example of a diatreme-hosted epithermal deposit in the Philippines

Acer Jian T. Figueroa [a,1,*], Jillian Aira S. Gabo-Ratio [a], Pearlyn C. Manalo [b], Ryohei Takahashi [b], Hinako Sato [b], Aljess B. Ramos [c]

[a] Rushurgent Working Group, National Institute of Geological Sciences, College of Science University of the Philippines, Diliman, Quezon City 1101, Philippines
[b] Graduate School of International Resource Sciences, Akita University, Akita 010-8502, Japan
[c] Benguet Corporation, Balatoc, Itogon, Benguet 2604, Philippines

ARTICLE INFO

Keywords:
Balatoc Diatreme
Acupan epithermal deposit
Fluid mixing

ABSTRACT

The Acupan epithermal gold deposit is one of the Philippines' largest gold camps, having produced over 200 t Au in the last century with average grades of ~ 6 g/t Au mostly from well-studied vein orebodies hosted by the Virac Granodiorite. However, vein and breccia mineralization (90/99 veins and GW orebodies, respectively) currently being mined in the northeastern portion of the Acupan deposit is hosted by the less-studied Balatoc Diatreme. This study demonstrates the role of the diatreme as a precursor to epithermal mineralization at Acupan, providing structural control in focusing the fluid flow along the diatreme margin. Mineralization in the Balatoc Diatreme formed across five mineralization stages. Stage I, the main gold mineralization stage, is characterized by gray quartz with pyrite + marcasite + arsenopyrite + electrum + sphalerite ± chalcopyrite. Stage II is typified by white quartz associated with pyrite + electrum + chalcopyrite. Stage III, a newly recognized stage for the Acupan gold deposit, is composed of clear quartz hosting pyrite + stibnite + chalcopyrite + galena + sphalerite + electrum (±pyrite + marcasite + arsenopyrite). Stage IV and Stage V are associated with calcite and gypsum, respectively, hosting trace amounts of pyrite and sphalerite.

Fluid inclusions hosted by Stage I and Stage II vein quartz revealed homogenization temperatures (T_h) ranging from 220 to 230 °C and 280 to 290 °C, respectively. The fluid inclusions in Stage III quartz breccia cement recorded bimodal homogenization temperatures, 230 to 240 °C and 280 to 290 °C. Fluid inclusion and textural evidence from Stage I quartz and Stage II quartz suggest boiling conditions during ore formation of veins transecting the Balatoc Diatreme. Fluid mixing, on the other hand, is proposed for the formation of the base-metal rich Stage III mineralization of the GW orebodies quartz cement. Pyrite and sphalerite $\delta^{34}S$ values (0.8 to 1.5 ‰) from Stage I to Stage IV veins and breccias indicate reduced ore-forming conditions in an H_2S-dominated system. Meanwhile, the negative $\delta^{34}S$ values (−1.6 to −1.5‰) measured from the pyrite of Stage V breccia, first reported in this study, imply partitioning of the heavier isotopes to the gypsum sulfate in an oxidizing environment and suggest possible spatial variations of sulfur isotope signatures across the Acupan epithermal vein system. This study emphasizes the significance of fluid mixing in diatreme-hosted epithermal deposits such as Acupan. The diatreme possibly provided pathways between the contrasting magmatic-hydrothermal and meteoric environments, resulting in ore precipitation.

1. Introduction

Since the recognition of the link between volcanic landforms and ore deposits in volcano-plutonic arcs (e.g. Sillitoe and Bonham, 1984), exploration activities immediately shifted to investigating the mineralization potential of volcanic landforms, especially diatremes. Diatremes

* Corresponding author.
E-mail address: ajtfigueroa@nigs.upd.edu.ph (A.J.T. Figueroa).
[1] Present affiliation: Ocean and Earth Science, National Oceanography Centre Southampton, University of Southampton Waterfront Campus, Southampton SO14 3ZH, United Kingdom.

https://doi.org/10.1016/j.oregeorev.2022.104826
Received 9 July 2021; Received in revised form 3 March 2022; Accepted 7 March 2022
Available online 8 March 2022

are large volcanic-hydrothermal breccia complexes, potentially hosting significant tonnage of precious and base metal deposits especially when occurring as a precursor to epithermal mineralization (e.g. Davies et al., 2008). The numerous diatreme breccia complexes associated with epithermal and porphyry deposits in the Philippines (e.g. Ruelo and Angeles, 2017; Kirwin, 2018, Fig. 1) make the country an ideal laboratory for diatreme-hosted deposits. A classic diatreme breccia complex is exemplified by the Balatoc Diatreme, a major host to the large Acupan epithermal vein system, within the world-class Baguio Mineral District in north Luzon.

The well-studied Acupan vein system is one of the world's largest epithermal systems in terms of contained gold, having produced over 200 t Au at 6 g/t average grade (United Nations Development Programme, 1987; Cooke and Bloom, 1990). The Acupan epithermal veins

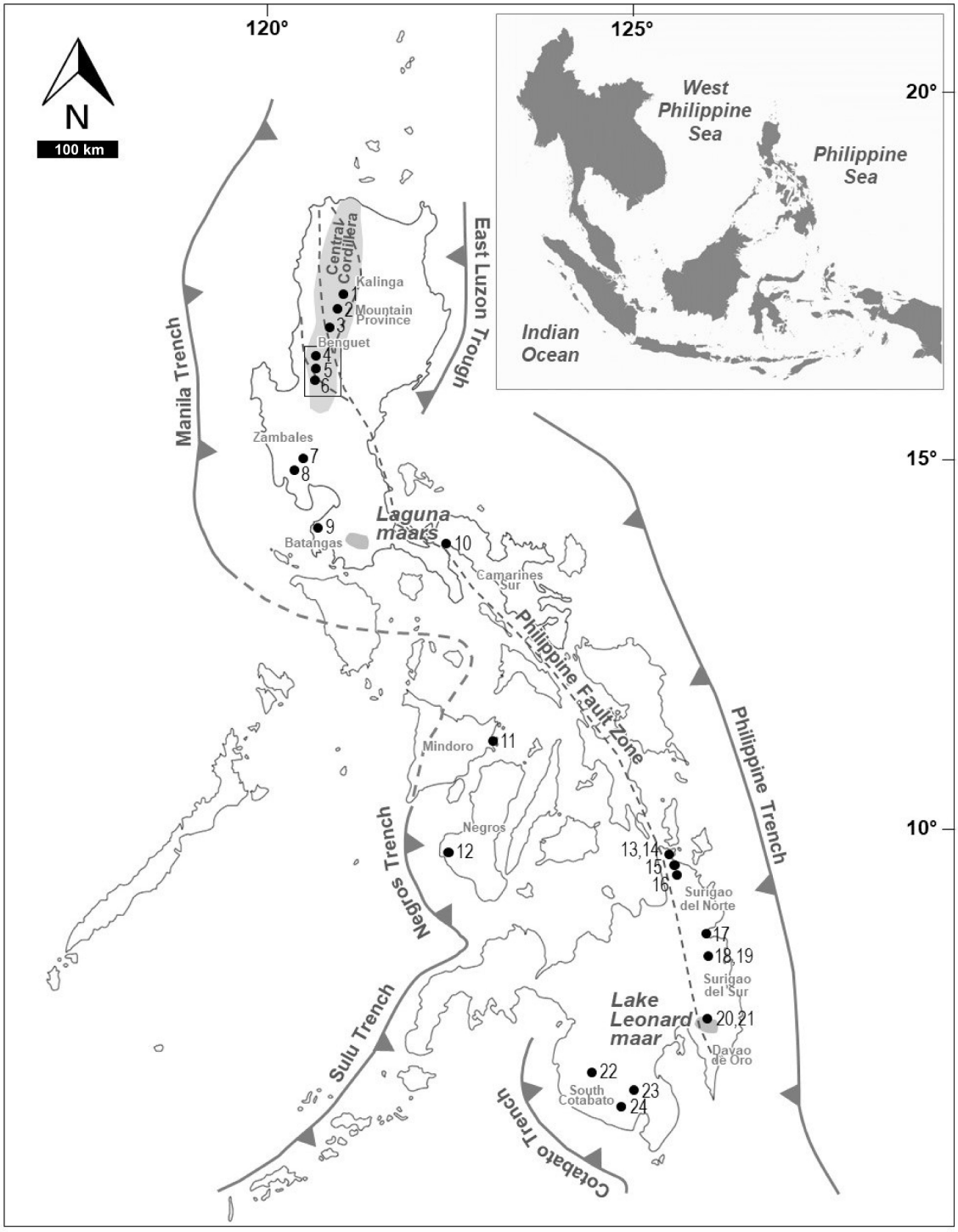

Fig. 1. Map of the Philippines showing major tectonic elements (subduction zones and fault zone) and localities of diatreme-hosted epithermal and porphyry deposits in the Philippines indicated by the black dots. Data from Ruelo and Angeles (2017) and Kirwin (2018). Maars (e.g. Laguna and Lake Leonard) are also marked in gray areas. Location of the Baguio Mineral District is indicated by the black rectangle. [1-Batong Buhay MCB, 2-Mainit, 3-Mankayan District (Lepanto, Far Southeast, Guinaoang, Suyoc), 4-Sto Niño, 5-Acupan, 6-Sto. Tomas II, 7-Pisumpan, 8-Dizon, 9-Panagsagan, 10-Del Gallego, 11-Pan de Azucar, 12-Bulawan, 13-Mapawa Motherlode, 14-Placer, 15-Boyongan, 16-Siana, 17-Tambis, 18-Red Mountain, 19-Co-O, 20-Magas, 21-Lumanggang, 22-Salatan, 23-Tampakan, 24-T'boli].

are primarily hosted by the Virac Granodiorite and the Balatoc Diatreme (Hedenquist et al., 2000; Cooke et al., 2011). Current production is from the 90 and 99 veins, and from hydrothermal breccia bodies, called GW orebodies, within the Balatoc Diatreme situated in the northeastern portion of the Acupan deposit. Despite numerous studies on the Acupan epithermal deposit, the breccia and vein mineralization of the Balatoc Diatreme remain inadequately documented and poorly understood.

Here, we present the mineralization characteristics and ore-forming conditions of the breccia and vein orebodies exclusively hosted by the Balatoc Diatreme constrained from paragenetic, fluid inclusion and sulfur isotope studies in an attempt to record ore-forming processes related to diatreme-hosted deposits and to demonstrate the significance of diatremes to ore formation in epithermal environments such as Acupan.

2. Geologic framework

2.1. Baguio Mineral District

The Baguio Mineral District (BMD) is one of the most well-documented mineralized areas in the Philippines (e.g. Bellon and Yumul, 2000; Polve et al., 2007; Yumul et al., 2008; Cooke et al., 2011; Fig. 2A). Situated within the Central Cordillera, it is host to numerous hydrothermal ore deposits and prospects attributed to several Pliocene to Pleistocene intrusion clusters (Waters et al., 2011).

Major deposits related to the Pliocene intrusive rocks include the Black Mountain porphyry Cu-Au (Sweet, 2012; Cao et al., 2018), the Mexico skarn (Waters et al., 2011) and the Thanksgiving skarn (Callow, 1967) in the western portion of the BMD (Fig. 2A). Meanwhile, Pleistocene porphyry copper mineralization in the BMD is represented by the Santo Tomas II deposit (Imai, 2001; Masangcay et al., 2018) and the adjacent Bumolo, Clifton, and Southwest prospects (Imai, 2001; Cirineo et al., 2021) in the southern portion. The youngest known porphyry copper deposit in the BMD is the Ampucao prospect (Cooke and Bloom, 1990; Cooke et al., 2011) in the east-central portion. Other porphyry prospects that have not yet been dated are located north of Ampucao, such as Nugget Hill and Chico (Waters et al., 2011) (Fig. 2A).

The BMD is also host to the two largest epithermal deposits in the Philippines, Antamok and Acupan-Sangilo (e.g. Sawkins et al., 1979; Waters et al., 2011; Jabagat et al., 2020; Fig. 2A). Other epithermal deposits in the central to northern portions of the BMD include Sierra Oro, Cal Horr, Atok Big Wedge, Kelly-Baco and Baguio Gold (Mitchell and Leach, 1991; Waters et al., 2011).

2.2. Acupan epithermal deposit

Among the numerous hydrothermal deposits in the BMD, the Acupan epithermal deposit is one of the most well-studied. It is the second largest gold resource within the BMD, next to the Antamok epithermal deposit (Fernandez and Damasco, 1979; Cooke et al., 1996). Since the beginning of underground mining operations of Benguet Corporation in 1929 until mine closure in 1993, more than 225 t Au have been extracted from composite banded quartz-carbonate veins and hydrothermal breccias of Acupan (Callow and Worley, 1965; Cooke et al., 2011). According to the United Nations Development Programme (UNDP) (1987), the average mining grade is ~ 6.1 g/t Au, with a cutoff grade of ~ 4.2 g/t, during the late 1980s. During the mid-1990s, Placer Dome Inc. reported a remaining bulk mining resource of 99 t Au. In

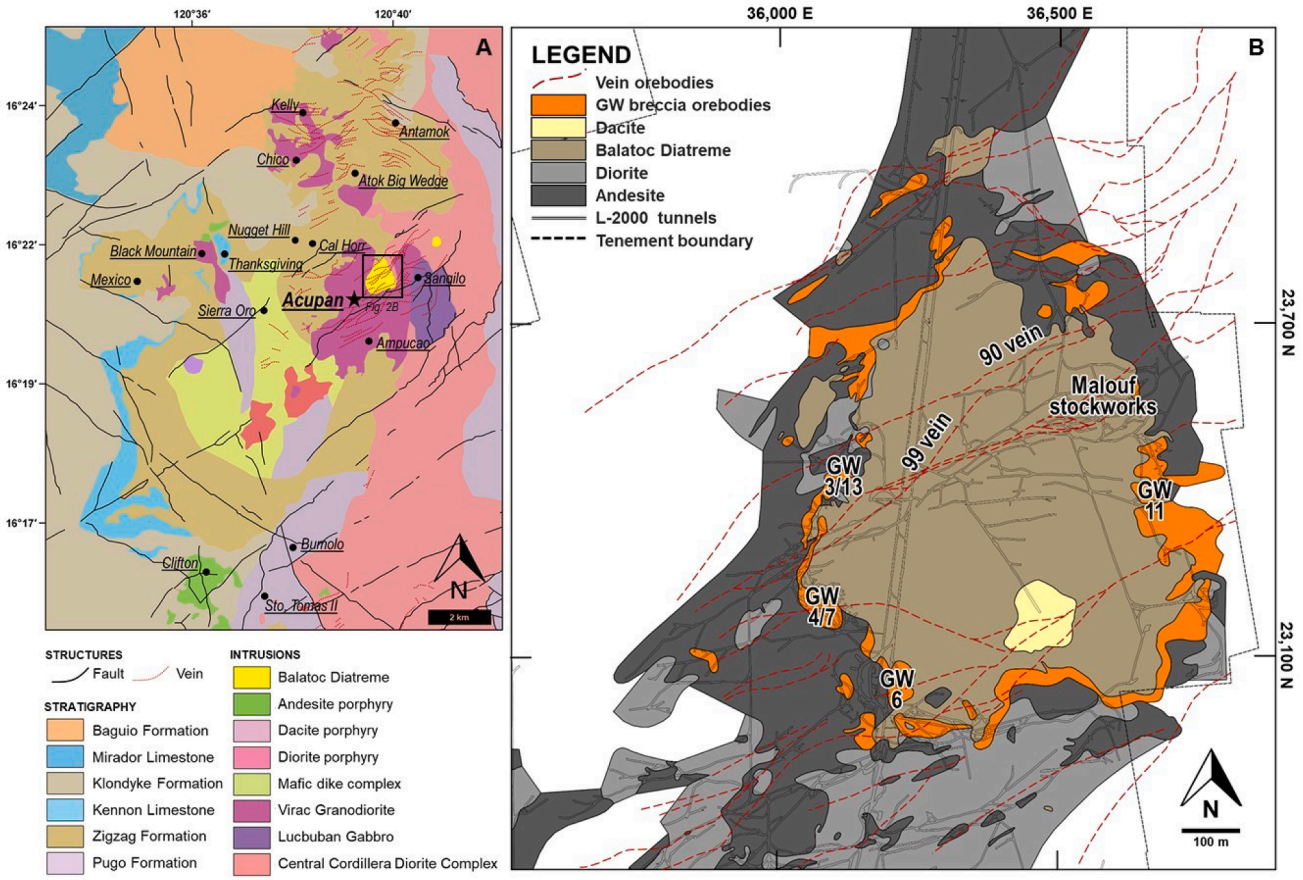

Fig. 2. (A) Geologic map of the BMD showing the locations of various hydrothermal deposits indicated by the black dots (Modified from Waters et al., 2011). (B) Geologic map (L-2000) of the Balatoc Diatreme and associated intrusive bodies. Epithermal veins (red dashed lines) and GW breccia orebodies (orange areas) investigated in this study are labelled. Access to these orebodies are through underground tunnels within the Benguet Corporation tenement.

2003, Benguet Corporation resumed operations in partnership with artisanal miners. In 2019, Benguet Corporation produced a total of 8,174.72 oz of Au with average grades of 6.18 g/t, milled from 41,151 t of ore (Benguet Corporation, 2020).

Mineralization at Acupan is characterized by numerous northeast-trending epithermal vein systems steeply dipping to the south. These veins are mainly hosted by the Virac Granodiorite in the central portion and the Balatoc Diatreme in the southern portions of the mine tenement. Early works on the Acupan epithermal deposit focused on telluride mineralogy (Callow and Worley, 1965) and limited fluid inclusion and stable isotope systematics (Sawkins et al., 1979). Both studies agree that initial deposition of auriferous gray quartz was followed by base metal sulfide-rich, coarse-grained white quartz.

A comprehensive study by Cooke and Bloom (1990) revealed a five-stage paragenetic sequence for the Acupan vein system, indicating early porphyry-related paragenetic stages (Stages I, II) which are overprinted by later epithermal paragenetic stages (Stages III, IV, V). Stage I veinlets are quartz-magnetite-chalcopyrite, while Stage II are crosscut veinlets of anhydrite-quartz-pyrite-chlorite (Stage II) veinlets crosscut. Stage III is characterized by fine-grained 'grey quartz' with abundant pyrite. An earlier study by Sawkins et al. (1979) suggested that this stage contains significant quantities of gold, occurring as inclusions in pyrite. Coarse-grained 'white quartz,' pyrite, adularia, K-mica and rhodochrosite dominate early stage IV deposition followed by calcite dominating the later Stage IV deposition (Cooke and Bloom, 1990). At this stage, free gold is associated with adularia (Callow and Worley, 1965). Lastly, there is no gold mineralization observed at anhydrite-dominated Stage V (Callow and Worley, 1965; Cooke and Bloom, 1990).

The paragenetic sequence was updated by Cooke et al. (1996) by distinguishing mineral assemblages for the Acupan epithermal veins. Adjacent wallrocks are altered to quartz-sericite-pyrite (K-mica). Along the margins of the crustiform banded veins are the early-formed gray quartz-cemented breccia (type B). Locally brecciated bands dominated by coarse-grained white quartz (type C) are the most abundant components of the veins in terms of volume. Calcite and anhydrite infills distinguish type D and type E bands, respectively. The rare type A chalcedony occurs as clasts within type B and C bands. In terms of gold association, electrum and Au-Ag tellurides were recognized with type B, C, and D bands.

Previously mentioned studies focused on the Acupan veins at the central and southern portions hosted by the Virac Granodiorite. Mineralization hosted by the Balatoc Diatreme at the northeastern portion of the deposit, however, remains poorly constrained.

2.3. *Balatoc Diatreme*

The Balatoc Diatreme discussed in this paper is equivalent to the Balatoc Plug of Leith (1938). It has been described as the main breccia mass of a classic explosion breccia by early works (e.g. Callow and Worley, 1965; Sawkins et al., 1979; Wolfe, 1986), but later on interpreted as a diatreme by De Guzman (1986) and succeeding studies.

Callow and Worley (1965) reported an average grade of 7.1 g/t for the vein oreshoots hosted by the Balatoc Diatreme. During the 1960′s, the Balatoc Diatreme contributed to 40% of monthly mine production

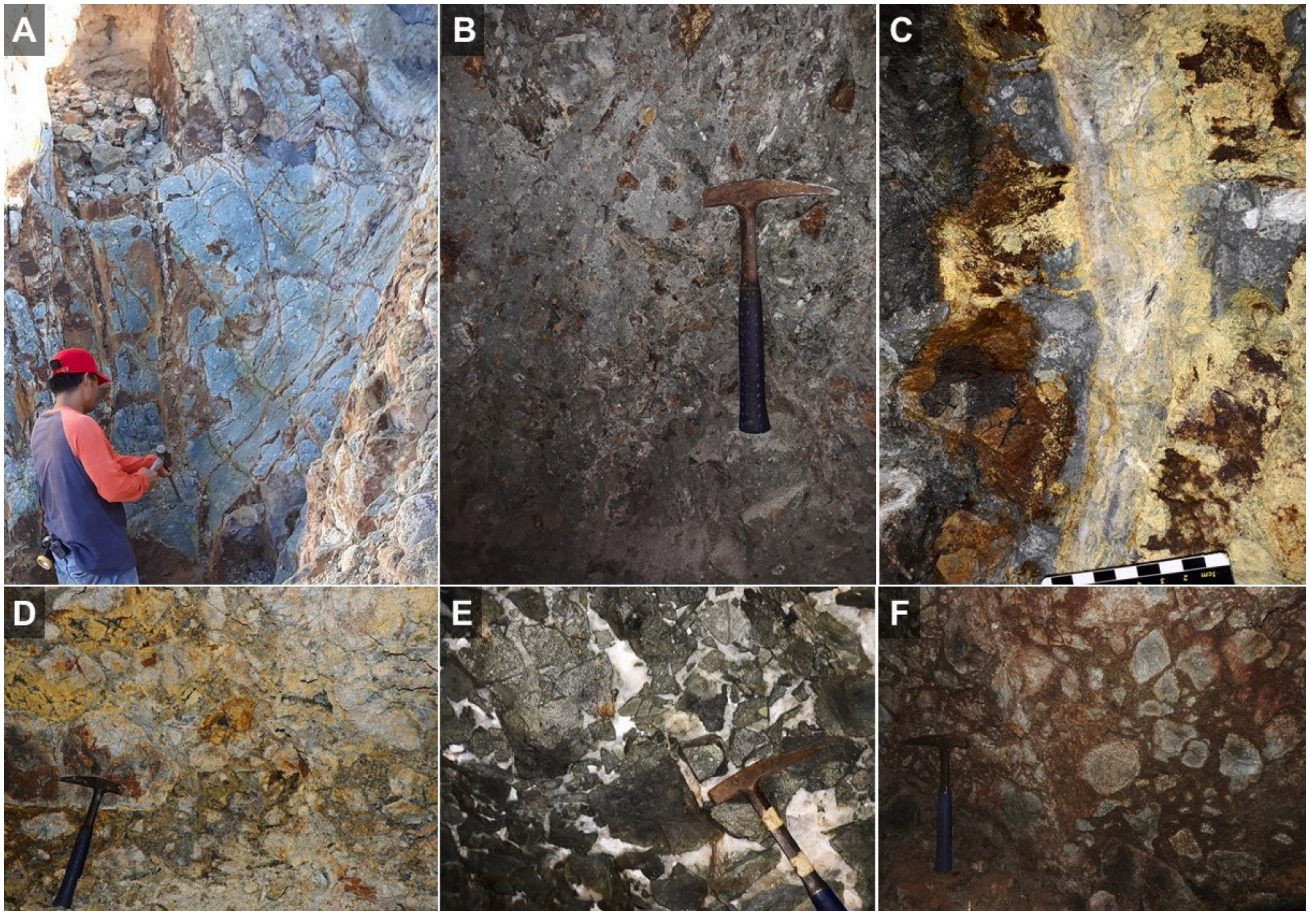

Fig. 3. Field occurrences of the Balatoc Diatreme and associated orebodies. (A) Surface and (B) underground exposures of the central portion of the Balatoc Diatreme. (C) Underground exposure of the 99 Vein steeply dipping to the south, cutting through the Balatoc Diatreme. (D-F) Underground exposures of the breccia orebodies with breccia classifications from Figueroa and Gabo-Ratio (2022): (D) GW 3/13: rotational, quartz-cemented diorite breccia with cross-cutting stibnite veinlets, (E) GW 11: mosaic, calcite-cemented andesite breccia, (F) GW 6: rotational, quartz-cemented polymict breccia.

capacity, producing 16,000 t Au with an average grade of 4 g/t Au. According to De Guzman (1986), the geologic potential of the oreshoots in the Balatoc Diatreme is estimated at 2.5 to 4 Mt at 3.8 g/t cut-off grade. A special report on the breccia orebody reported an average tenor of 1.3 g/t Au, with individual assays ranging from 2.2 to 37.0 g/t Au (Ilagan, 1981). Subsequently, De Guzman (1986) reported gold grades ranging from 4 to 30 g/t Au for both the vein and breccia-stockwork ore shoots.

The Balatoc Diatreme is composed of rounded clasts of diorite and andesite, with rare charcoal fragments, set in a matrix of fine-grained components (Callow and Worley, 1965; Sawkins et al., 1979; Fig. 2B, 3A, B). The matrix is composed of comminuted dacite, andesite and angular fragments of quartz with alteration minerals, epidote and chlorite (Sawkins et al., 1979). The abundance and size of the fragments present in the matrix varies within the Balatoc Diatreme (Sawkins et al., 1979). The central portion of the Balatoc Diatreme contains smaller and more scattered fragments, whereas the margins contain larger and more closely-spaced fragments. This was later designated by De Guzman (1986) to be the 'young plug' and 'old plug' of the Balatoc Diatreme, respectively. However, this spatial change in breccia internal organization is interpreted as a function of breccia facies change in a single event attributed to its proximity to the surrounding intrusive rocks (Figueroa and Gabo-Ratio, 2022).

The Balatoc Diatreme is host to various orebodies exhibiting three mineralization styles (vein, breccia and stockwork). Vein orebodies transecting the Balatoc Diatreme include the 90 and 99 veins, which are relatively thinner compared to their Acupan vein counterparts hosted by the Virac Granodiorite. Breccia orebodies, on the other hand, occur where the veins coincide with the margins of the Balatoc Diatreme. Callow and Worley (1965) referred to these diatreme breccia-hosted mineralization as 'GW breccia pipe' which is equivalent to the GW orebodies referred to in this paper (Fig. 2B). The GW breccia orebodies range from clast-supported to matrix-supported and from monomictic to polymictic breccias with diorite and andesite clasts (Fig. 3D–F). These breccia orebodies are cemented by clear quartz, calcite and gypsum hosting variable amounts of sulfides. Detailed descriptions of these breccia orebodies are included in a separate manuscript (Figueroa and Gabo-Ratio, 2022). Veins (e.g. 90 and 99 veins in Fig. 2B) transecting the Balatoc Diatreme also become stockwork veins at the northeastern rim of the diatreme (De Guzman, 1986; Cooke et al., 2011). This stockwork mineralizationis referred as the Malouf deposit and is beyond the scope of this study.

3. Methodology

Samples of the vein and breccia orebodies hosted by the Balatoc Diatreme were collected from underground workings at mine levels L-2000 (796 m.a.s.l.) and L-1875 (820 m.a.s.l.) within the Benguet Corporation tenement (PC-ACMP-002-CAR). Due to safety and security reasons, some areas were not accessible at the time of sampling. Epithermal veins (90 and 99 veins), GW 6 and GW 11 orebodies were collected at mine level L-2000, while GW 3, GW 4, GW 7 and GW 13 were collected at mine level L-1875. It should be noted that some GW orebodies with similar breccia characteristics are grouped together (e.g. Figueroa and Gabo-Ratio, 2022) and will be referred to as GW 3/13 (GW 3 and GW 13) and GW4/7 (GW 4 and GW 7) in the succeeding discussions.

Thin and polished sections of representative samples were observed using an Olympus BX53-P polarizing microscope housed at the National Institute of Geological Sciences, University of the Philippines. Qualitative SEM-EDS analysis of selected polished sections was also conducted for further mineral identification using the JEOL JXA-8800R electron probe microanalyzer at the Faculty of International Resource Sciences, Akita University, Japan.

Bulk Au and Ag concentrations of representative samples of each vein mineralization stage were also analyzed. Quartz vein and breccia fragments were lightly crushed in an iron mortar; fractions were further pulverized using an agate mortar and pestle. Powdered samples were processed via acid digestion methods using HF, $HClO_4$ and aqua regia. Au and Ag contents were measured using an Agilent Technologies 7500 Series inductively coupled plasma - mass spectrometer (ICPMS) at the Faculty of International Resource Sciences, Akita University, Japan.

Doubly polished sections with 150 to 200 μm thickness of vein quartz samples and breccia quartz related to gold deposition were subjected to fluid inclusion petrography and microthermometry. Freezing, ice-melting and homogenization temperatures (T_h) were measured using a Linkam THM 600 heating-freezing stage attached to a Nikon Eclipse LV100N POL polarizing microscope housed at the Faculty of International Resource Sciences, Akita University, Japan. Salinity (in wt% NaCl eq.) of the observed fluid inclusions were calculated using the equation of Bodnar (1993).

Sulfur isotope analysis was carried out at Akita University, Japan. Sulfides (e.g. pyrite and sphalerite) were separated via handpicking under the binocular microscope. Decomposition of the sulfides (20 mg) was done by adding 20 mL concentrated HNO_3 and 2 mL Br_2 at 95 °C. The sample solution was then evaporated to dryness. The resulting residue was dissolved in 10 mL 6 M HCl and was subsequently diluted to 100 mL. Any undissolved matter was filtered. The resulting solution was passed through a cation exchange column to avoid coprecipitation with other cations. Ten milliliters of 10% $BaCl_2{\cdot}2H_2O$ was added to the eluent to precipitate $BaSO_4$. Retrieved $BaSO_4$ was packed with V_2O_5 in tin foil (Yanagisawa and Sakai, 1983). Packed samples were loaded into the automatic sampler and combusted in a quartz tube at 1,020 °C using a Thermo Fisher Flash 2000 Elemental Analyzer. The produced SO_2 gas was separated via gas chromatography. Sulfur isotopic ratios were measured using a Thermo Fisher Scientific Delta V Advantage isotope ratio monitoring mass spectrometer at Akita University. IAEA NBS-127 ($\delta^{34}S_{CDT} = 20.30$ ‰), IAEA SO-6 (–34.10 ‰), and IAEA SO-5 (0.50 ‰) are the standards used in the analysis (Halas and Szaran, 2001). Analytical precision is better than 0.2 ‰.

4. Results

4.1. Ore mineralogy and paragenesis

Five paragenetic stages are identified for the breccia and vein orebodies within the Balatoc Diatreme (Fig. 4). Unlike their epithermal vein counterparts hosted by the Virac Granodiorite, these types do not exhibit cross-cutting relationships. Instead, a transitional sequence of older mineral assemblage closer to the walls and younger towards the central portion of the veins and breccia spaces is more pronounced. The first three paragenetic stages are defined by three quartz varieties from the oldest to youngest: gray quartz (Stage I), white quartz (Stage II) and clear quartz (Stage III). Stage I gray quartz and Stage II white quartz are abundantly recognized in the 90 and 99 veins (Fig. 5A). Stage III clear quartz is more common in the GW orebodies (Fig. 5B). Late-stage infilling of carbonates (Stage IV) and sulfates (Stage V) was also observed for the breccia orebodies (Fig. 5C–E).

Stage I is characterized by crustiform textures of gray quartz, with brecciated portions along vein margins (Fig. 5A). This paragenetic stage is correlated to Stage III of Cooke and Bloom (1990) and Type B vein of Cooke et al. (1996). The color is attributed to microcrystalline quartz textures and abundance of sulfides; chloritized clasts and mineral fragments were also observed in brecciated portions of the veins (Fig. 6A). De Guzman (1986) suggested that the gray quartz was formed via replacement of the original gouge material by silica along fractures.

Occurring as inclusions within Stage I quartz, ore minerals of Stage I vein infill include pyrite + marcasite + arsenopyrite + electrum + sphalerite ± chalcopyrite. Stage I is richest in gold in the form of electrum hosted by marcasite (Fig. 6B–D). Subhedral marcasite replacing pyrite was also observed with Stage I vein infill (Fig. 6B). Minor subhedral sphalerite, some exhibiting chalcopyrite disease, are included

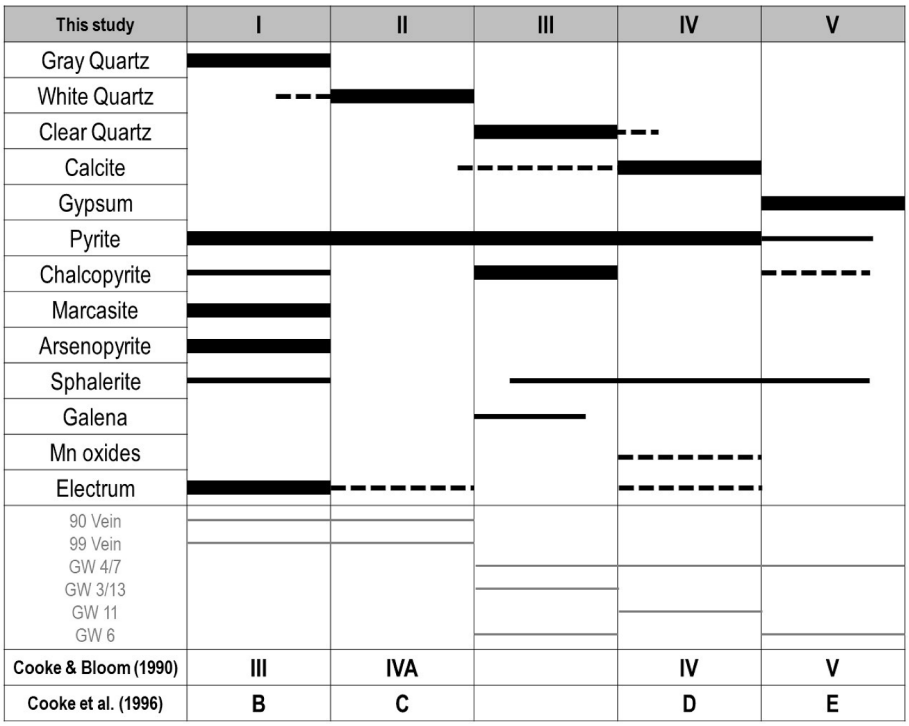

Fig. 4. Paragenetic sequence of the breccia and vein mineralization hosted by the Balatoc Diatreme. Thick and thin solid lines represent major and minor minerals, respectively. Dashed lines indicate trace amounts of the mineral per mineralization stage.

within euhedral pyrite crystals (Fig. 6E). Zonation of marcasite, pyrite and arsenopyrite was also observed for Stage I vein infill (Fig. 6F, G).

Veins hosted by the Balatoc Diatreme show a gradational sequence of Stage I infill near the wallrock to Stage II infill near the central portion of the veins (Fig. 5A). White quartz, exhibiting bladed and macrocrystalline textures (Fig. 5A; Fig. 6H), dominates Stage II of the paragenetic sequence. This stage may be related to Stage IVa of Cooke and Bloom (1990) and Type C vein of Cooke et al. (1996). Stage II is characterized by abundant coarse-grained euhedral pyrite and late-stage subhedral chalcopyrite hosted within quartz (Fig. 6I, J). Gold mineralization for Stage II occurs as electrum hosted by pyrite (Fig. 6I).

Both Stage I and Stage II were observed in the 90 and 99 vein orebodies. These are also the two stages richest in gold. Geochemical analysis of veins samples show that the 90 vein contains up to 3.7 ppm Au and up to 8.0 ppm Ag, while the 99 vein contains a maximum of 14.8 ppm Au and 14.6 ppm Ag.

Stage II white quartz also occurs as breccia infill in all the GW orebodies observed in this study (GW 3/13, 4/7, 6, 11; Fig. 3D–F). In several breccia orebodies, a gradational relationship from Stage II white quartz to Stage III clear quartz were observed in the breccia infill. Unlike other paragenetic stages, Stage III clear quartz of this study has not been described by previous studies. Stage III clear quartz exhibits comb textures (Fig. 7A), with few occurrences of feathery textures. Ore minerals of Stage III breccia infill include pyrite + chalcopyrite + galena + sphalerite + electrum. These ore minerals were observed adjacent to breccia clasts and along fractures within the clasts. Early-formed coarse-grained euhedral galena exhibits interpenetrating boundaries with coarse-grained subhedral pyrite (Fig. 7B, C); euhedral cubic pyrite included within late-stage chalcopyrite was also observed (Fig. 7D). Minor amounts of fine-grained electrum were observed to be hosted by coarse-grained chalcopyrite (Fig. 7E). Stage III breccia infill is also defined by sphalerite occurring as inclusions within galena (Fig. 7C). Late-stage stibnite veinlets were observed to cut the breccia infill of GW 3/13. Undulatory extinction and twinning were observed for the stibnite crystals in this paragenetic stage (Fig. 7F).

Gold concentrations of the GW orebodies (GW 3/13, 4/7, 6) with Stage III breccia infill are generally lower compared to those of the veins. The GW 4/7 and the GW 6 orebodies record 1.5 ppm Au and 1.2 ppm Au, respectively. Meanwhile, GW 3/13 has Au content reaching up to 4.2 ppm.

The Stage IV breccia infill of the GW 11 orebody is dominated by bladed calcite and is partially replaced by quartz (Fig. 5C, D, 7G). This paragenetic stage is correlated to Stage IVb of Cooke and Bloom (1990) and Type D vein infill of Cooke et al. (1996). Stage IV is characterized by minor amounts of pyrite with sphalerite inclusions (Fig. 7H). Similar to Stage III ore minerals, these ore minerals were observed adjacent to breccia clasts and along fractures within the clasts. Gold-bearing minerals for this stage were not observed under the microscope. However, GW 11 has Au concentrations reaching up to 12.6 ppm. Cross-cutting relationships and gradational contacts with earlier paragenetic stages were not observed for this paragenetic stage due to the limited occurrence.

Stage V is characterized by gypsum hosting trace amounts of pyrite and sphalerite, minor amounts of which were observed at the GW 4/7 and GW 6 orebodies. This may be related to the Stage V of Cooke and Bloom (1990) and Type D vein infill of Cooke et al. (1996). Similar to Stage IV calcite, Stage V gypsum also exhibits limited occurrences as cement to the GW orebodies.

4.2. Fluid inclusion systematics

Fluid inclusions hosted by Stage I quartz vein from the 90 and 99 veins are dominantly composed of liquid and liquid-rich biphase fluid inclusions (Fig. 8A). Most are regular-shaped with size ranging from 5 to 30 μm. Irregular-shaped, solitary vapor-rich fluid inclusions, 10 to 20 μm in size, are less common in Stage I quartz (Fig. 8B). Liquid-rich fluid inclusions homogenize to liquid within temperatures between 220 and 230 °C; salinity values measured from these fluid inclusions range from 1.9 to 4.0 wt% NaCl eq. Vapor-rich fluid inclusions, on the other hand, homogenize to liquid at 230 to 480 °C and record salinity values reaching up to 8.7 wt% NaCl eq., higher compared to those recorded from the liquid-rich fluid inclusions (Fig. 9A, B).

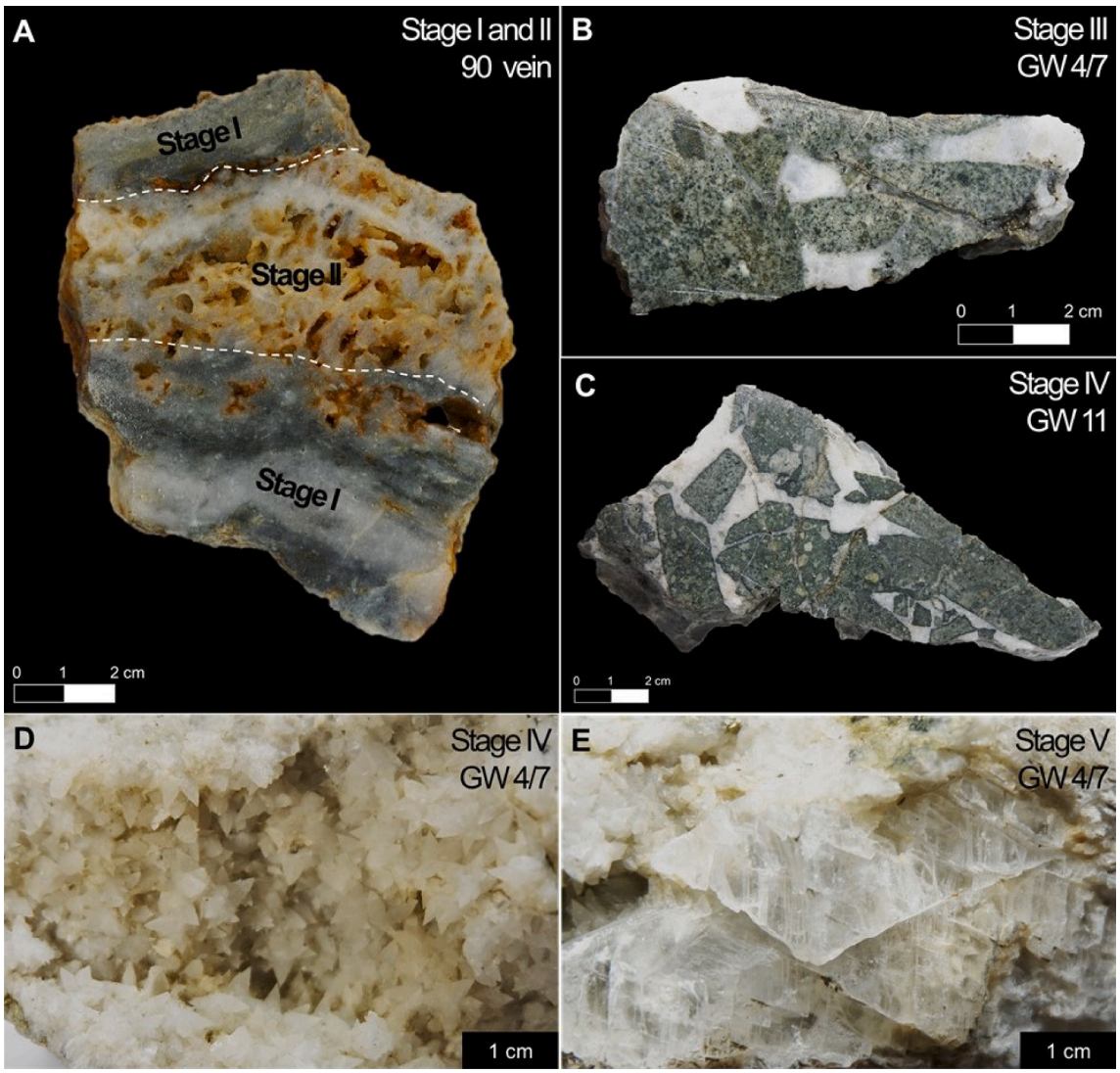

Fig. 5. Hand sample photos of the Balatoc orebodies. (A) Stage I and Stage II vein showing a transitional sequence from gray quartz to white quartz from the wallrock towards the center of the vein. (B) Stage III clear quartz cementing the diorite clasts of the GW 4/7 orebody. (C) Stage IV calcite cementing porphyritic andesite clasts of the GW 11 orebody. (D) Occurrence of drusy calcite in Stage IV breccia infill of the GW 4/7 orebody. (E) Stage V selenite in the breccia cement of the GW 4/7 orebody.

Stage II quartz from the 90 and 99 veins also host liquid-rich and vapor-rich fluid inclusions. Regular-shaped liquid-rich biphase fluid inclusions range from 5 to 60 μm in size (Fig. 8C), while irregular-shaped solitary vapor-rich vapor–liquid inclusions are 10 to 20 μm in size (Fig. 8D). Stage II liquid-rich fluid inclusions homogenize to the liquid phase at 280 to 290 °C. Vapor-rich liquid inclusions hosted by Stage II quartz, on the other hand, homogenize to liquid and vapor at 170 to 480 °C. Salinity values measured from Stage II liquid-rich fluid inclusions range from 2.1 to 4.3 wt% NaCl eq., while vapor-rich fluid inclusions record salinity values reaching up to 13.1 wt% NaCl eq (Fig. 9C, D).

Fluid inclusions hosted by Stage III quartz breccia cement are dominantly composed of liquid and liquid-rich fluid inclusions (5 to 60 μm) with rare vapor-rich fluid inclusions (30 to 60 μm) (Fig. 8E–H). Due to the open space characteristics of the other breccia orebodies, the reported microthermometric measurements in this paper are limited to the quartz breccia cement of the GW 4/7. Regular-shaped liquid-rich biphase fluid inclusions (Fig. 8E, F, I) record two modes of homogenization temperatures, 230 to 240 °C and 280 to 290 °C and salinity content ranging from 1.1 to 6.0 wt% NaCl eq. Irregular-shaped vapor-rich fluid inclusions (Fig. 8G, H) record homogenization temperature range (248 to 418 °C) and salinity range (4.7 to 5.9 wt% NaCl eq.) (Fig. 9E, F).

4.3. Sulfur isotope systematics

Table 1 shows the measured $\delta^{34}S_{CDT}$ values from sulfides of the Balatoc breccia and vein orebodies across mineralization stages. Compared to $\delta^{34}S_{CDT}$ values of the Acupan veins reported by Cooke et al. (2011), $\delta^{34}S_{CDT}$ values of pyrite and sphalerite from the Balatoc veins and breccias are generally lower (Fig. 10). The $\delta^{34}S_{CDT}$ of pyrite from Stage I to Stage IV all have positive values, ranging from 0.8 ‰ to 1.5 ‰. On the contrary, the $\delta^{34}S_{CDT}$ values of pyrite and sphalerite of Stage V from GW 4/7 breccia orebody are all negative. The $\delta^{34}S_{CDT}$ values from the first four paragenetic stages are near 1‰, then a sudden decrease in the $\delta^{34}S_{CDT}$ values at Stage V was recorded.

5. Discussion

5.1. Ore-forming processes

Epithermal environments allow the development of boiling (e.g.,

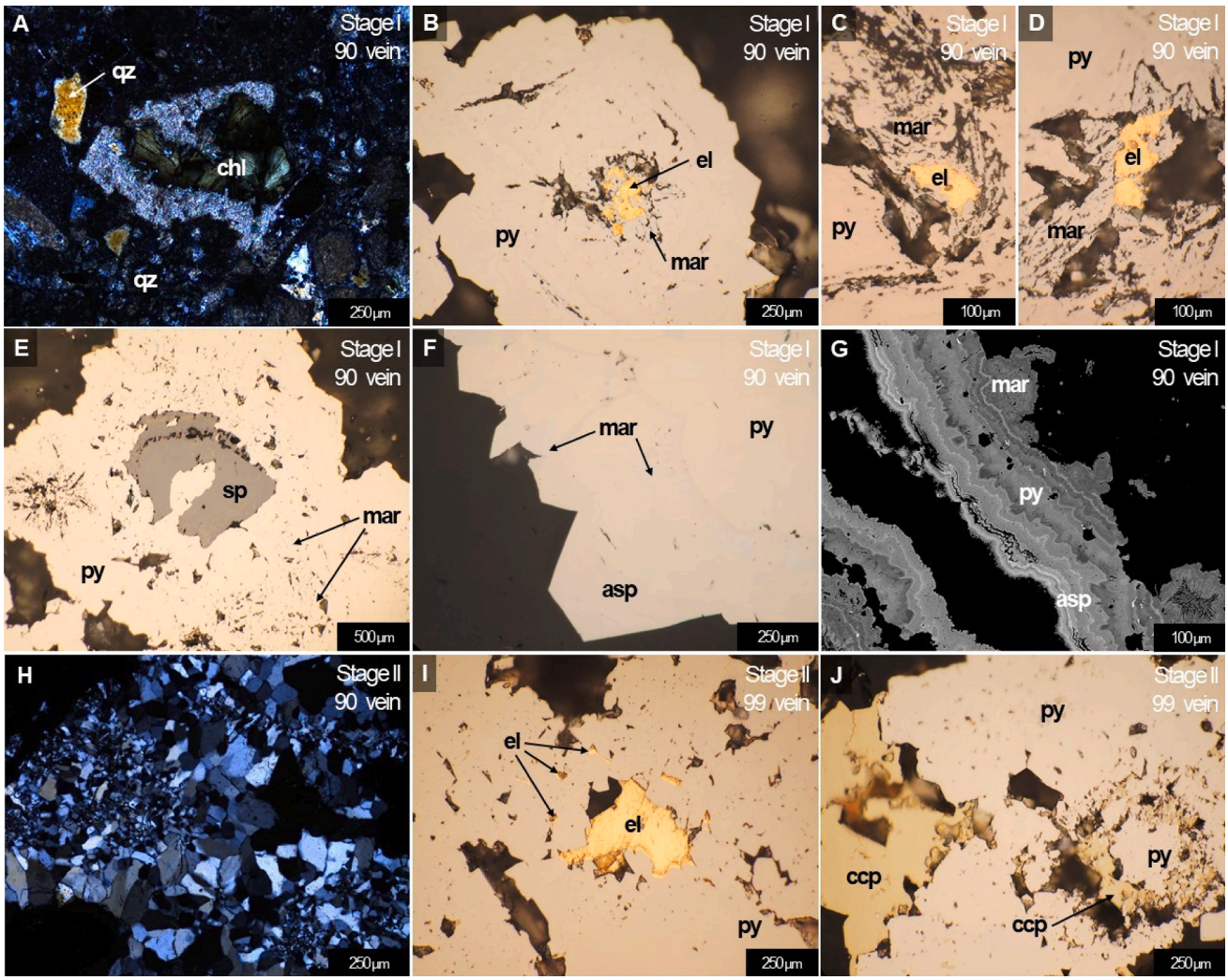

Fig. 6. Photomicrographs of ore and gangue minerals from the Balatoc epithermal veins. (A) Brecciated portion of Stage I gray quartz from the 90 Vein showing chloritized clasts and quartz fragments. (B-D) Occurrences of electrum hosted by marcasite and pyrite. (e) Sphalerite inclusions in marcasite and pyrite. (F, G) Photomicrograph and backscatter secondary electron image of zonation of marcasite, pyrite and arsenopyrite. (H) Macrocrystalline quartz textures of the Stage II white quartz from the 90 Vein showing portions of microcrystalline quartz. (I) Electrum hosted within pyrite crystals. (J) Early-formed pyrite with late-stage chalcopyrite. [asp: arsenopyrite, ccp: chalcopyrite, chl: chlorite, el: electrum, mar: marcasite, py: pyrite, sp: sphalerite, qz: quartz].

Drummond and Ohmoto, 1985; Spycher and Reed, 1989) and mixing (e.g. Plumlee and Hayba, 1986) conditions which are conducive to precious and base metal precipitation. In this study, evidence for both processes were observed for the Balatoc Diatreme-hosted breccia and vein orebodies based on ore-gangue textures and fluid inclusion data.

5.1.1. *Evidence for boiling*

The presence of crustiform and bladed quartz textures observed in the 90 and 99 veins suggests boiling conditions for Stage I and Stage II precious metal deposition (e.g. Moncada et al., 2012). Moreover, coexistence of liquid-rich and vapor-rich fluid inclusions observed from Stage I and Stage II vein quartz is also likely due to boiling. This is further supported by additional fluid inclusion evidence such as the skewness of the T_h histograms at high temperatures and the steep slope of the salinity-T_h trend from Stage I and II fluid inclusions (Hedenquist and Henley, 1985) (Fig. 9A, B).

The minimum depth of ore deposition below the paleowater table for Stage I and Stage II was estimated using the hydrostatic boiling point curves for brines of constant composition by Haas (1971). As shown in Fig. 11, a boiling condition at hydrostatic conditions for Stage I quartz from the 90 vein (796 m a.s.l.) is estimated to occur at around 260 m below the assumed paleowater table. Stage I quartz from the 99 vein and Stage II quartz from the 90 vein, both collected at 796 m a.s.l., depict boiling conditions under lithostatic pressure. This may explain the increase in the homogenization temperatures recorded from Stage I to Stage II.

5.1.2. *Evidence for fluid mixing*

Compared to Stage I and Stage II mineralization, salinity and homogenization temperature arrays recorded from Stage III breccia cement quartz suggest mixing of low-temperature, low-salinity fluids and high-temperature, moderate-salinity fluids (Fig. 9E, F) similar to the diatreme-hosted Kelian gold deposit, East Kalimantan, Indonesia (Davies et al., 2008) and Roșia Montană deposit, South Apuseni Mountains, Romania (Wallier et al., 2006).

Using the estimated paleodepth of ore formation from Stage I and Stage II, samples from the Stage III quartz breccia cement were also plotted on the diagram of Haas (1971) of hydrostatic boiling point curves for brines of constant composition. Paleodepth estimates for Stage III quartz from the GW 4/7 (820 m a.s.l) at around 230 m beneath the assumed paleowater table (Fig. 11). The bimodal distribution from Stage III quartz breccia cement may be attributed to variable pressure conditions, from hydrostatic to lithostatic, via temporal silica sealing (e.g. Roedder and Bodnar, 1980; Takahashi et al., 2007). It is suggested

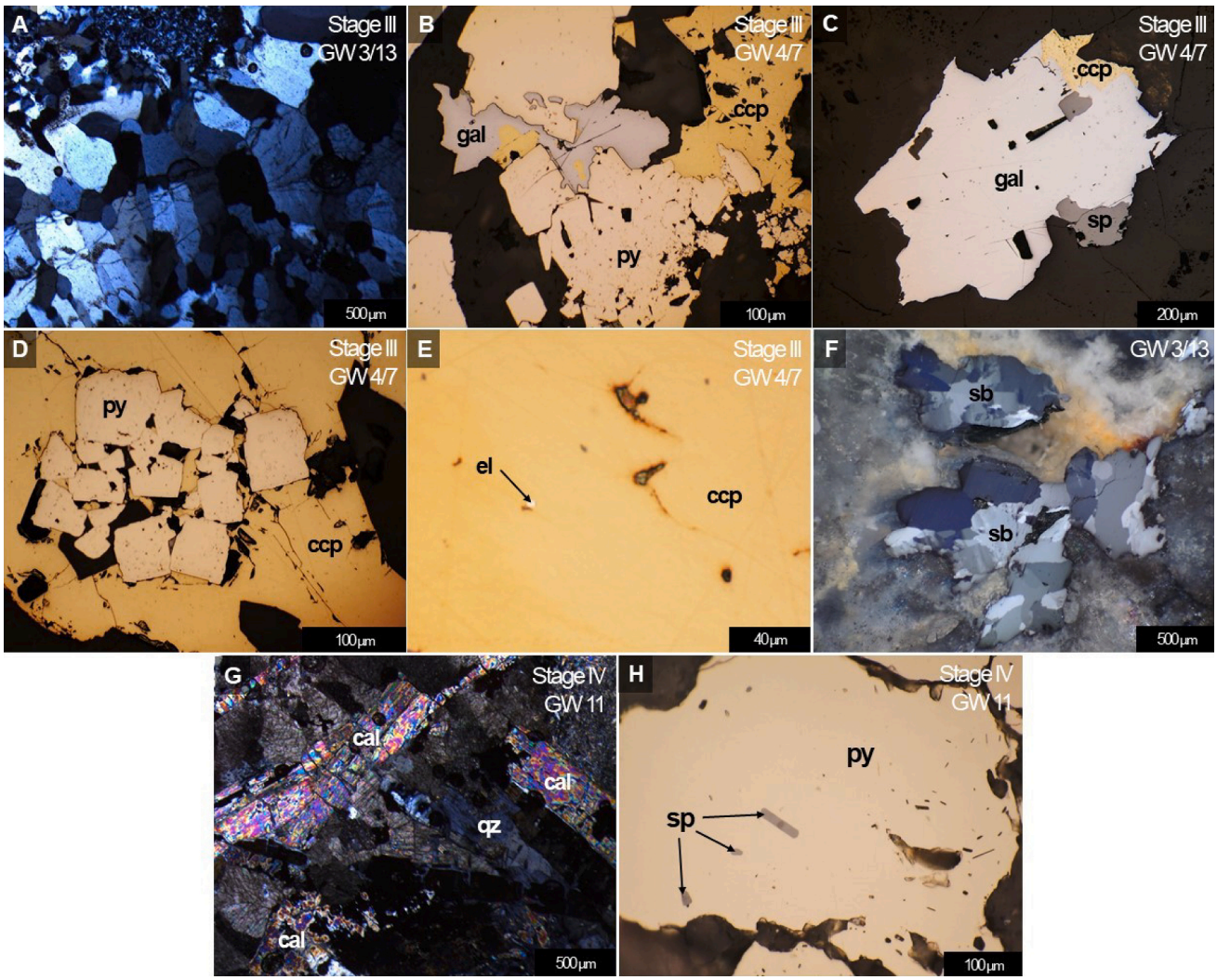

Fig. 7. Photomicrographs of ore and gangue minerals from the GW breccia orebodies. (A) Comb textures of Stage III clear quartz the GW 3/13 orebody. (B) Early-formed pyrite and galena with late-stage chalcopyrite. (C) Sphalerite inclusions within galena with late-stage chalcopyrite. (D) Euhedral pyrite cubes included within late-stage chalcopyrite. (E) Electrum hosted within chalcopyrite. (F) Stibnite crystals showing anisotropism and undulatory extinction. (G) Bladed calcite textures of the Stage IV breccia infill from the GW 11 orebody replaced by quartz. (H) Sphalerite inclusions within pyrite. [asp: arsenopyrite, cal: calcite, ccp: chalcopyrite, el: electrum, gal: galena, mar: marcasite, py: pyrite, sp: sphalerite, sb: stibnite, qz: quartz].

that Stage III mineralization occurred after temporary closure of the shallower portions of the conduit forming an environment between lithostatic and hydrostatic pressure conditions. Subsequent mixing of low-temperature (230 to 240 °C) and high-temperature (280 to 290 °C) hydrothermal fluids occurred which may also explain the rare occurrence of vapor-rich fluid inclusions in Stage III quartz.

5.1.3. Implications to boiling and mixing zones at the Balatoc Diatreme

The relative position of orebodies within the hydrothermal systems often reflects the dominant ore-forming processes responsible for the genesis of large epithermal deposits such as Acupan (e.g. Cooke and Simmons, 2000). Generally, boiling zones are confined to areas of maximum upflow, while mixing conditions are limited to the margins and outflow zones of epithermal systems.

In this study, boiling is inferred to be the dominant mechanism for ore formation for Stage I and Stage II, mineralization stages associated with the vein orebodies. Therefore, we suggest that large structural features in Acupan became upflow zones and provided controls for a decrease in pressure as the rising liquids are becoming saturated with vapor. However, mixing is not disregarded as an ore-forming mechanism for Stage I and Stage II due to the presence of high salinity values from fluid inclusion microthermometric measurements.

Meanwhile, mixing is proposed to be the dominant ore-forming mechanism from Stage III onwards primarily based on the bimodal distribution of homogenization temperature histogram for Stage III quartz (Fig. 9F). For the Acupan epithermal deposit, we propose that the Balatoc Diatreme acted as an internal barrier and significantly influenced the divergent lateral spread of the fluids towards the margin of the diatreme where the breccia orebodies are located. This resulted in the formation of outflow zones where deep high-temperature, high-salinity hydrothermal fluids possibly influenced by magmatic water may interact with shallow low-temperature, low-salinity meteoric fluids. In addition, mixing zones are generally restricted to late-stage collapse of hydrothermal systems where steam-heated waters descend into the mineralizing system (Cooke and Simmons, 2000). Such conditions produce late-stage barren carbonate- or sulfate-dominated mineralization which may explain the mineralization characteristics observed for Stage IV and Stage V.

5.2. Physico-chemical conditions

Changes in temperature and redox conditions throughout the

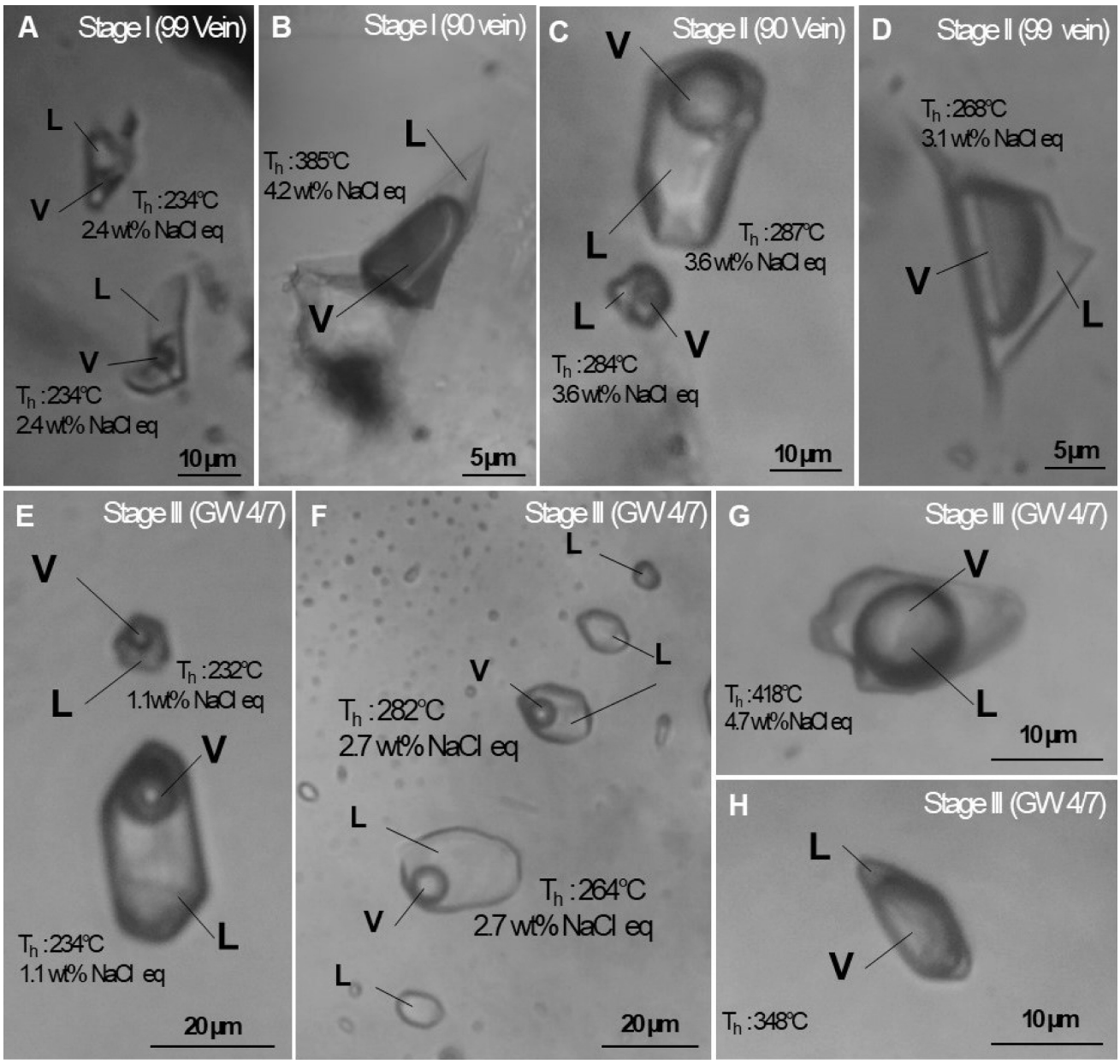

Fig. 8. Fluid inclusions in quartz vein and breccia cement of the Balatoc orebodies. (A, B) Liquid-rich (A) and vapor-rich (B) fluid inclusions hosted by Stage I quartz from the 90 and 99 veins. (C, D) Liquid-rich (C) and vapor-rich (D) fluid inclusions hosted by Stage II quartz from the 90 and 99 veins. (E-H) Liquid-rich (E, F) and vapor-rich (G, H) fluid inclusions hosted by Stage III breccia cement from the GW 4/7 orebody. (I) Stage III liquid and liquid-rich fluid inclusions from the GW 4/7 orebody. [L: liquid, V: vapor].

hydrothermal evolution of the Balatoc Diatreme-hosted orebodies were also recorded in this study.

5.2.1. Temperature of formation

The mineralogy of Stage I vein infill, characterized by quartz deposition associated with abundant electrum, pyrite, marcasite and arsenopyrite, suggests a reducing environment during the initial stages of mineralization at Balatoc. Formational temperature of this stage is estimated at 220 to 230 °C based on Stage I fluid inclusions. Anomalously high homogenization temperatures recorded, however, are attributed to the heterogeneous trapping of both the liquid and vapor phases in fluid inclusions due to boiling.

Stage II is also characterized by precious metal mineralization and quartz deposition. The mineral assemblage of Stage II also indicates a reducing environment. The temperature of the mineralizing event increased during this stage to between 280 and 290 °C. This temperature increase is attributed to a shift from hydrostatic to lithostatic pressure conditions as discussed in the previous section.

Marking the onset of base metal deposition, Stage III mineralization recorded a bimodal distribution of homogenization temperatures, 230 to 240 °C and 280 to 290 °C. Such records are interpreted as a result of fluid mixing being the dominant ore-forming mechanism as previously discussed from fluid inclusion data.

The presence of stibnite is also observed for the breccia and vein orebodies at Balatoc, similar to the Hishikari and the Okuchi gold deposits in Japan (Shimizu, 2017). Stibnite may indicate location at the peripheral portions or shallower portions of epithermal gold systems (Morteani et al., 2011; Schwarz-Schampera, 2014). This mineral also indicates reduced ore-forming conditions. At Balatoc, stibnite mineralization probably occurred between Stages III and V based on cross-cutting relationships observed at the GW 3/13 breccia orebody.

Estimates of formational temperature for Stages IV and V are inferred

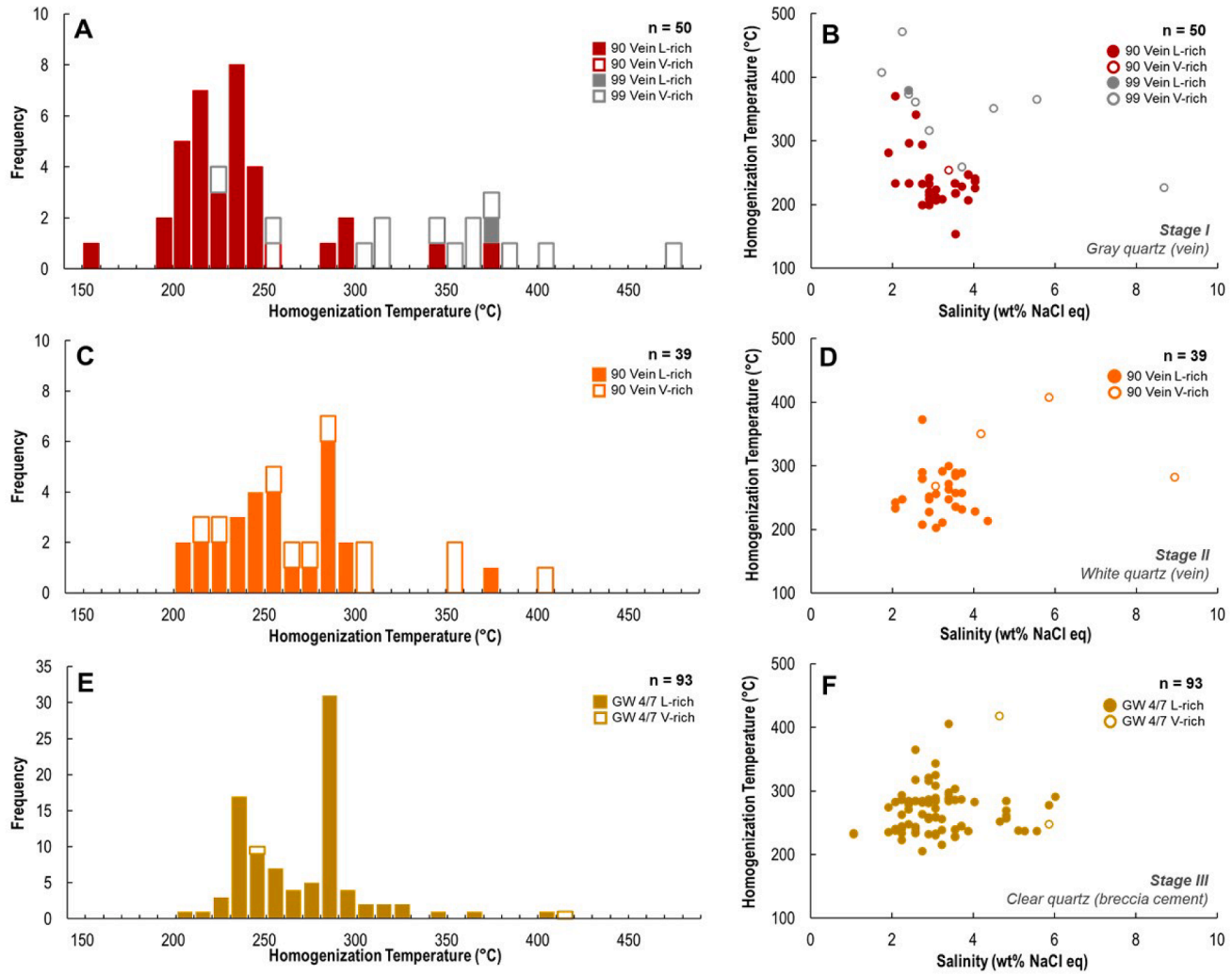

Fig. 9. Fluid inclusion microthermometry data from Stage I and Stage II quartz. (A, C, E) Homogenization temperature histograms of Stage I (A), Stage II (C) and Stage III (E) fluid inclusions in quartz. (B, D, F) Homogenization temperature vs salinity diagrams of Stage I (B), Stage II (D) and Stage III (F) fluid inclusions in quartz.

Table 1
Sulfur isotope data from the Balatoc orebodies across mineralization stages.

Sample Name	Mineral	Stage	$\delta^{34}S_{CDT}$
99Vn-py1	pyrite	Stage I	1.092
99Vn-py2	pyrite	Stage II	1.048
99Vn-py4	pyrite	Stage II	1.245
90Vn-py1	pyrite	Stage II	1.479
GW3/13-py1	pyrite	Stage III	0.80
GW6-py1	pyrite	Stage III	1.24
GW11-py1-1	pyrite	Stage IV	1.46
GW11-py1-2	pyrite	Stage IV	1.51
GW4/7-py1	pyrite	Stage V	−1.49
GW4/7-py2-1	pyrite	Stage V	−1.50
GW4/7-sp1-1	sphalerite	Stage V	−1.56
GW4/7-sp1-2	sphalerite	Stage V	−1.49
GW4/7-sp2	sphalerite	Stage V	−1.57

from previous studies. Cooke and Bloom (1990) reported a homogenization temperature range of 148 to 310 °C for Stage IVb calcite of the Acupan veins, correlatable to Stage IV in this study. Gypsum, on the other hand, is stable at temperatures less than ca. 123 °C. It is therefore proposed that the presence of calcite and gypsum in Stage IV and Stage V mineralization, respectively, indicate a progressive decrease in temperature towards the waning stages of the evolution of the deposit.

5.2.2. Redox conditions

Positive $\delta^{34}S_{CDT}$ values of pyrite and sphalerite from Stage 1 through Stage IV suggest reduced ore-forming conditions at the Balatoc Diatreme, similar to the sulfur isotope dataset of Cooke et al. (2011). In contrast, negative $\delta^{34}S_{CDT}$ values of pyrite, are indicative of oxidized ore-forming conditions during Stage V mineralization. The sudden decrease in the $\delta^{34}S_{CDT}$ values from Stage IV to Stage V is, therefore, attributed to a change from reducing to oxidizing environments.

Compared to the $\delta^{34}S_{CDT}$ values reported for the veins at the central and southern portions of Acupan, the Balatoc Diatreme-hosted breccia and vein orebodies recorded relatively lower $\delta^{34}S_{CDT}$ values. Moreover, negative $\delta^{34}S_{CDT}$ values reported for Stage V mineralization of the Balatoc Diatreme have not been documented by previous studies on the Acupan epithermal deposit. Such relationship warrants further investigation on the spatial variations of sulfur isotope signatures within the Acupan epithermal vein system.

5.3. Fluid sources

Epithermal ore-forming environments are characterized by dominance of meteoric fluids based on stable isotope studies (e.g., Nash, 1972; O'Neil and Silberman, 1974; Kamilli and Ohmoto, 1977; Buchanan, 1981). However, the contribution of magmatic-hydrothermal fluids in these environments is not disregarded (e.g. Hedenquist and Lowenstern, 1994; Simmons, 1995; Sillitoe and Hedenquist, 2003).

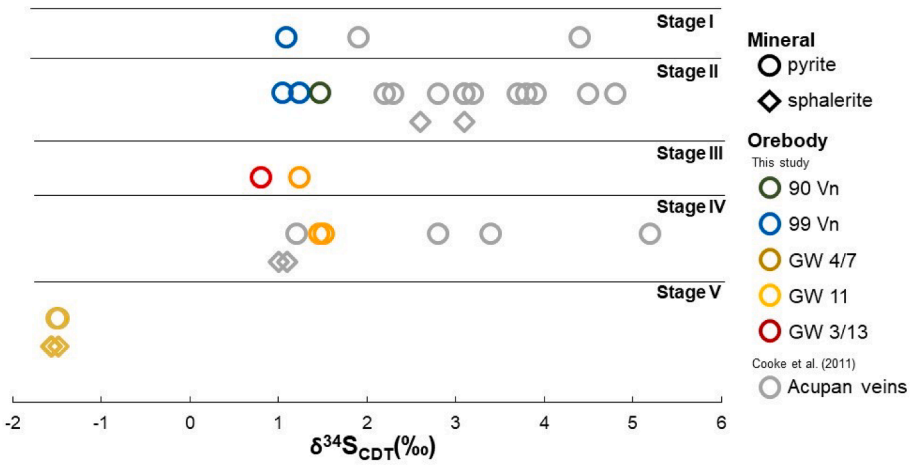

Fig. 10. Sulfur isotope data from the Balatoc orebodies across mineralization stages. Sulfur isotope data from the Acupan veins hosted by the Virac Granodiorite by Cooke et al. (2011) are plotted for comparison.

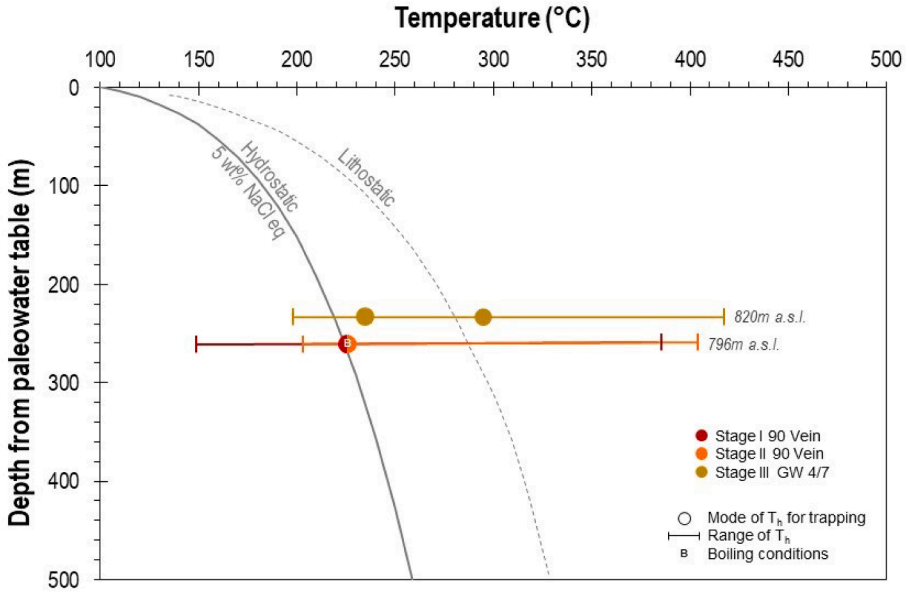

Fig. 11. Boiling depth–temperature diagrams. Boiling point curves are given for lithostatic conditions (2.7 g/cm^3) and 2.0 wt% NaCl equivalent solution under hydrostatic conditions (after Haas, 1971). Fluid inclusion microthermometry data from Stage I to Stage III are plotted for interpretation.

5.3.1. Evidence for meteoric water input

In this study, homogenization temperature ranges (230° to 240 °C) and low salinity values (1 to 2 wt% NaCl eq.) measured from fluid inclusions hosted by the Balatoc vein quartz and breccia cement are suggestive of a meteoric water component in the ore-forming fluids for the Balatoc Diatreme. Oxygen isotopic evidence from the epithermal vein counterparts hosted by the Virac Granodiorite also suggest convection of meteoric waters on the formation of the Acupan deposit (Sawkins et al., 1979; Cooke et al., 2011).

5.3.2. Evidence for magmatic fluid influence

Presence of vapor-rich fluid inclusions, anomalously high temperatures and moderate salinity values (greater than 10 wt% NaCl eq.) in Stage I and Stage II suggest contributions from fluids of possibly magmatic in origin during the formation of the Balatoc epithermal veins. This is further supported by sulfur isotope data recorded by the Balatoc orebodies, with $\delta^{34}S_{CDT}$ values near 0‰ (Ohmoto and Rye, 1979; Field and Fifarek, 1985), suggesting presence of magmatic sulfur in the mineralizing system. Moreover, the narrow range of $\delta^{34}S_{CDT}$ values from Stage I to Stage IV suggests that H_2S was the predominant sulfur species in the ore-forming fluids during the first four stages of mineralization. On the other hand, the dominant aqueous sulfur species for Stage V mineralization is SO_4^{2-}, which is consistent with the presence of sulfates in this paragenetic stage.

While evidence from fluid inclusion and sulfur isotope data demonstrate the predominance of meteoric input for the fluids which formed the breccia and veins at Balatoc, the presence of deeply-circulated fluids with possible magmatic origin in the mineralizing system is still not disregarded. Such interpretation is further supported by fluid inclusion evidence for fluid mixing of high-temperature, moderate salinity fluids and low-temperature, low salinity meteoric fluids throughout variable pressure conditions.

6. Genetic model

Diatreme volcanism and brecciation: The Plio-Pliocene history of the BMD is characterized by diatreme volcanism controlled by faults associated with a Pliocene deformation event (Fernandez and Damasco,

1979). At Balatoc, diatreme volcanism is estimated at 1.0 Ma based on fission track dating study of the diatreme by Japan International Cooperation Agency (JICA) (1983). Such volcanism triggered phreatomagmatic brecciation at the northeastern portions of the Acupan epithermal deposit, enhancing permeability and providing an environment favorable for precious and base metal deposition in the Balatoc breccia and vein orebodies (Fig. 12).

Early-stage precious metal mineralization: Early stages of mineralization (Stage I and Stage II) in Balatoc are characterized by dominance of precious metals associated with quartz. Textural and fluid inclusion evidence demonstrated by the veins transecting the Balatoc Diatreme point to boiling conditions. Similar conditions are responsible for the formation of the Acupan epithermal veins hosted by the Virac Granodiorite.

Late-stage base metal mineralization: The Balatoc Diatreme restricted fluid flow into the adjacent host rocks, focusing the hydrothermal brecciation along the outline of the diatreme. These became sites for fluid mixing of deeply circulated fluid and shallow meteoric fluid producing base metals associated with quartz (Stage III).

Post-mineralization events: A shift from reducing to oxidizing conditions produced the barren stages dominated by carbonates (Stage IV) and sulfates (Stage V). We consider that significant erosion after 0.65 Ma, based on the mineralization age of Acupan by Aoki et al. (1993), subsequent to diatreme emplacement due to the absence of preserved maar or tuff rings and exposure of some of the veins at the surface.

7. Insights to role of diatremes in epithermal environments

Diatremes make excellent exploration targets for precious and base metals especially when formed prior to the main stages of hydrothermal mineralization in epithermal environments (e.g. Sillitoe and Bonham, 1984; Tămaș and Milési, 2002). In this study, the Balatoc Diatreme served as a precursor to the Acupan epithermal gold mineralization. It provided major structural controls in the genesis of the deposit which may possibly explain the varying styles of mineralization observed at Balatoc. The contrast in the competence between the Balatoc Diatreme and the Virac Granodiorite, the major hosts to the Acupan epithermal deposit, resulted into differing vein widths in different parts of the deposit. The gold-rich Balatoc veins (90 and 99 veins) are relatively thinner compared to their vein counterparts hosted by the Virac Granodiorite. In addition, the poorly-lithified characteristic of the Balatoc Diatreme allowed the formation of the stockwork zones (Malouf deposit) at the northeastern portions of the diatreme. More importantly, enhanced permeability along the outline of the Balatoc Diatreme focused fluid flow along the margin of the diatreme, producing important tonnages of ore in the form of the GW breccia orebodies (Fig. 12).

Diatremes may also be considered as bridges between the deep magmatic-hydrothermal systems and shallow epithermal environments. Such characteristics allows the interaction between multiple fluid sources (e.g. magmatic and meteoric) in the entire hydrothermal system, attaining conditions conducive for mixing zones (e.g. Davies et al., 2008). In this study, fluid mixing is emphasized as an integral process in diatreme-hosted mineralization based on observations from the various GW breccia orebodies of the Balatoc Diatreme. Finally, we suggest that the Balatoc Diatreme is a possible link between early porphyry and subsequent epithermal mineralization observed at Acupan, producing pathways for fluids from these two contrasting environments (Fig. 12).

8. Conclusions

The breccia and vein orebodies hosted in the Balatoc Diatreme record the diversity of ore-forming processes and physico-chemical conditions in the genesis of large epithermal deposits such as Acupan. Mineralization at Balatoc is divided into five paragenetic stages. The first two stages (Stage I and Stage II) represent early stages of precious metal mineralization formed at boiling conditions. Meanwhile, Stage III clear quartz, not previously described, represents the dominance of base metal mineralization produced via fluid mixing. Lastly, the latter stages (Stage IV and Stage V) are relatively barren of precious metal mineralization compared to the earlier paragenetic stages.

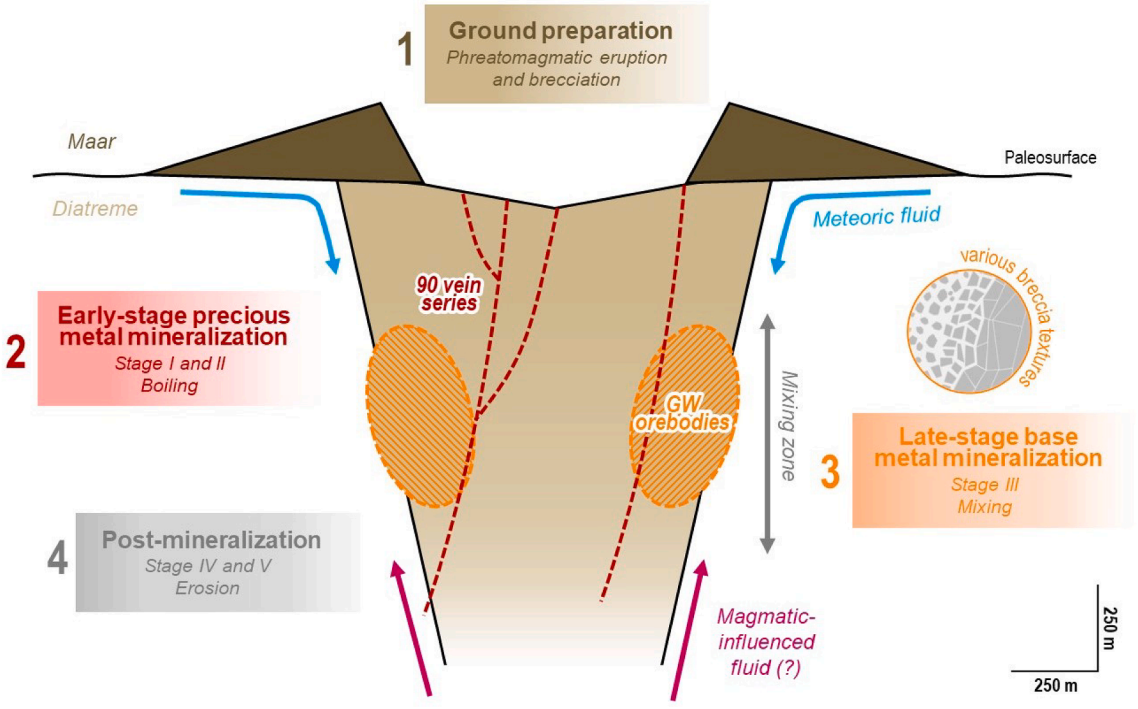

Fig. 12. Simplified illustration of the mineralization events associated with the Balatoc vein and GW breccia orebodies: 1) diatreme volcanism accompanied by brecciation; 2) formation of precious metal-rich veins cutting the diatreme; 3) mineralization of the base metal-rich GW breccia orebodies; 4) relatively barren mineralization and subsequent erosion.

Fluid inclusion and sulfur isotope data of the Balatoc orebodies suggest prevalence of meteoric water input in a dominantly reduced ore-forming environment across variable pressure conditions. However, involvement of fluids possibly of magmatic origin is suggested during the formation of the Balatoc orebodies, reiterating the importance of fluid mixing in diatreme-hosted mineral deposits. Moreover, late-stage oxidizing ore-forming conditions based on sulfur isotope data, first reported in this study, suggest spatial variations of sulfur isotope signatures within the Acupan epithermal vein system.

Ultimately, this study demonstrates the role of the Balatoc Diatreme as a structural control in focusing the fluid flow along the margin of the diatreme and as a pathway between the contrasting magmatic and meteoric environments producing mixing zones conducive for precious and base metal precipitation.

Declaration of Competing Interest

The authors declare that they have no known competing financial interests or personal relationships that could have appeared to influence the work reported in this paper.

Acknowledgements

The authors wish to acknowledge the logistical support provided by the Benguet Corporation. The authors are deeply indebted to Prof. Huayong Chen (co-Editor-in-Chief) and three anonymous reviewers for their editorial inputs and suggestions. Discussions with the members of the Rushurgent Working Group (UP-NIGS) and the Economic Geology Research Group (Akita University) are highly appreciated. This work was funded through a research grant awarded to J.A.S. Gabo-Ratio by the University of the Philippines System Balik PhD Program (OVPAA-BPhD-2016-05). This work was also partially funded by the Continuous Operational and Outcomes-based Partnership for Excellence in Research and Academic Training Enhancement (COOPERATE) which is administered by the Office of International Linkages, University of the Philippines. Funding support through the NIGS Research Grant 2018 awarded to A.J.T. Figueroa is also gratefully acknowledged.

Funding statement

This work was funded through a research grant awarded to J.A.S. Gabo-Ratio by the University of the Philippines System Balik PhD Program (OVPAA-BPhD-2016-05). This work was also partially funded by the Continuous Operational and Outcomes-based Partnership for Excellence in Research and Academic Training Enhancement (COOPERATE) which is administered by the Office of International Linkages, University of the Philippines.

References

Aoki, M., Comsti, E.C., Lazo, F.B. and Matsuhisa, Y., 1993, Advanced argillic alteration and geochemistry of alunite in an evolving hydrothermal system at Baguio, northern Luzon, Philippines: Shigen-Chishitsu, 43, 155–164.

Bellon, H., Yumul Jr., G.P., 2000. Mio-Pliocene magmatism in the Baguio Mining District (Luzon, Philippines): age clues to its geodynamic setting. Comptes Rendus de l'Académie des Sciences - Series IIA - Earth and Planetary Science 331 (4), 295–302.

Benguet Corporation, 2020. Amended Annual Report 2019 (SEC Form 17-A), Retrieved from http://benguetcorp.com/wp-content/uploads/2020/07/2019-Amended-Annual-Report-SEC-Form-17A.pdf.

Bodnar, R.J., 1993. Revised equation and table for determining the freezing point depression of H_2O-NaCl solutions. Geochimica et Cosmochimica Acta 57 (3), 683–684.

Buchanan, L.J., 1981. Precious metal deposits associated with volcanic environments in the southwest. Arizona Geol. Soc. Digest 14, 237–262.

Callow, K.J., Worley, J., 1965. The occurrence of telluride minerals at the Acupan gold mine, Mountain Province, Philippines. Econ. Geol. 60, 251–268.

Callow, K.J., 1967. The geology of the Thanksgiving mine, Baguio district, Mountain province, Philippines. Econ. Geol. 62, 472–481.

Cao, M., Hollings, P., Cooke, D.R., Evans, N.J., McInnes, B.I., Qin, K., Li, G., Sweet, G., Baker, M., 2018. Physicochemical processes in the magma chamber under the Black Mountain porphyry Cu-Au deposit, Philippines: Insights from mineral chemistry and implications for mineralization. Econ. Geol. 113, 63–82.

Cirineo, A.V.L., Imai, A., Takahashi, R., Baluda, R.P., Oliveros, N.C., Maglambayan, V.B., Luis, R.R.C., Faustino, M.L.M., Almadin, J., 2021. Overprinting porphyry-type veinlets on the intrusive rocks and phreatomagmatic breccias in the Southwest prospect, southwestern Sto. Tomas II (Philex), Baguio District, Philippines. Resour. Geol. 71, 1–40.

Cooke, D.R., Deyell, C.L., Waters, P.J., Gonzales, R.I., Zaw, K., 2011. Evidence for magmatic-hydrothermal fluids and ore-forming processes in epithermal and porphyry deposits of the Baguio district, Philippines. Econ. Geol. 106 (8), 1399–1424.

Cooke, D.R., Bloom, M.S., 1990. Epithermal and subjacent porphyry mineralization, Acupan, Baguio district, Philippines: A fluid-inclusion and paragenetic study. J. Geochem. Explor. 35 (1-3), 297–340.

Cooke, D.R., Simmons, S.F., 2000. Characteristics and genesis of epithermal gold deposits. Rev. Econ. Geol. 13, 221–244.

Cooke, D.R., McPhail, D.C., Bloom, M.S., 1996. Epithermal gold mineralization, Acupan, Baguio District, Philippines; geology, mineralization, alteration, and the thermochemical environment of ore deposition. Econ. Geol. 91, 243–272.

Davies, A.G.S., Cooke, D.R., Gemmell, J.B., van Leeuwen, T., Cesare, P., Hartshorn, G., 2008. Hydrothermal breccias and veins at the Kelian gold mine, Kalimantan, Indonesia: Genesis of a large epithermal gold deposit. Econ. Geol. 103 (4), 717–757.

De Guzman, M.T., 1986. Geology and mineralization of the Balatoc diatreme, Acupan Mine. Unpublished report, Benguet, p. 66.

Drummond, S.E., Ohmoto, H., 1985. Chemical evolution and mineral deposition in boiling hydrothermal systems. Econ. Geol. 80, 126–147.

Fernandez, H.E., Damasco, F.V., 1979. Gold deposition in the Baguio gold district and its relationship to regional geology. Econ. Geol. 74, 1852–1868.

Field, C.W., Fifarek, R.H., 1985. Light-stable isotope systematics in epithermal systems. Rev. Econ. Geol. 2, 99–128.

Figueroa, A.J.T., Gabo-Ratio, J.A.S., 2022. Breccia characteristics and classification of the GW orebodies, Balatoc Diatreme, Philippines: Insights to breccia facies and distribution across diatremes. Resour. Geol. 72, e12282. https://doi.org/10.1111/rge.12282.

Haas, J.L., 1971. The effect of salinity on the maximum thermal gradient of a hydrothermal system at hydrostatic pressure. Econ. Geol. 66, 940–946.

Halas, S., Szaran, J., 2001. Improved thermal decomposition of sulfates to SO_2 and mass spectrometric determination of $\delta^{34}S$ of IAEA SO-5, IAEA SO-6 and NBS-127 sulfate standards. Rapid Commun. Mass Spectrometry 15, 1618–1620.

Hedenquist, J.W., Henley, R.W., 1985. The importance of CO_2 on freezing point measurements of fluid inclusions: evidence from active geothermal systems and implications for epithermal ore deposition. Econ. Geol. 80, 1379–1406.

Hedenquist, J.W., Lowenstern, J.B., 1994. The role of magmas in the formation of hydrothermal ore deposits. Nature 370 (6490), 519–527.

Hedenquist, J.W., Arribas Jr, A., Gonzalez-Urien, E., 2000. Exploration for epithermal gold deposits. Rev. Econ. Geol. 13, 45–77.

Ilagan, P.E., 1981, Special report on GW-type breccia zone along Balatoc Plug South Rim Project. Unpublished report, 3 p.

Imai, A., 2001. Generation and evolution of ore fluids for porphyry Cu-Au mineralization of the Santo Tomas II (Philex) deposit, Philippines. Resour. Geol. 51, 71–96.

Jabagat, K.D., Gabo-Ratio, J.A., Queaño, K.L., Yonezu, K., Dimalanta, C.B., Lee, Y.-H., Yumul, G.P., 2020. Petrogenetic constraints on magma fertility in the Baguio Mineral District, Philippines: Probing the mineralization potential of the igneous host rocks in the Sangilo epithermal deposit. Ore Geol. Rev. 125, 103703.

Japan International Cooperation Agency (JICA), 1983. Report on Acupan-Itogon Geothermal Development. Tokyo, Unpublished report, First phase survey, p. 94.

Kamilli, R.J., Ohmoto, H., 1977. Paragenesis, zoning, fluid inclusion, and isotopic studies of the Finlandia vein, Colqui district, central Peru. Econ. Geol. 72, 950–982.

Kirwin, D.J., 2018. Diatremes Associated with Epithermal and Porphyry Systems in the Philippines [abs]: Geological Society of the Philippines, Geological Convention: Building the Country, Securing the Future: The Role of Filipino Geoscientists, Manila, Philippines, 2018. Abstract Volume.

Leith, A., 1938. Geology of the Baguio gold district: Philippine Department of Agriculture and Commerce. Technical Bull. 5, 55 p.

Masangcay, B.S.M., Luis, R.R.C., Irorita, K.I.N., Cellona, G.D., Maglambayan, V.B., Baluda, R.P., 2018. Mineralization controls of the gold-rich zone below Santo Tomas II porphyry copper-gold deposit, Tuba, Benguet, Philippines. J. Geol. Soc. Philippines 74, 1–13.

Mitchell, A.H.G., Leach, T.M., 1991. Epithermal gold in the Philippines: Island arc metallogenesis, geothermal systems and geology. Academic Press.

Moncada, D., Mutchler, S., Nieto, A., Reynolds, T.J., Rimstidt, J.D., Bodnar, R.J., 2012. Mineral textures and fluid inclusion petrography of the epithermal Ag-Au deposits at Guanajuato, Mexico: Application to exploration. J. Geochem. Explor. 114, 20–35.

Morteani, G., Ruggieri, G., Möller, P., Preinfalk, C., 2011. Geothermal mineralized scales in the pipe system of the geothermal Piancastagnaio power plant (Mt. Amiata geothermal area): a key to understand the stibnite, cinnabarite and gold mineralization of Tuscany (central Italy). Mineralium Deposita 46 (2), 197–210.

Nash, J.T., 1972. Fluid inclusion studies of some gold deposits in Nevada. US Geological Survey Professional Paper 800, C15–C19.

Ohmoto, H., Rye, R.O., 1979. Isotopes of sulfur and carbon. In: Barnes, H.L. (Ed.), Geochemistry of hydrothermal deposits, 2nd ed. Wiley, New York, pp. 506–567.

O'Neil, J.R., Silberman, M.L., 1974. Stable isotope relations in epithermal Au-Ag deposits. Econ. Geol. 69, 902–909.

Plumlee, G.S., Hayba, D.O., 1986. Preliminary chemical modeling of epithermal processes at Creede, Colorado: the role of fluid mixing as an ore deposition mechanism. In: Proceedings of the Workshop on Geochemical Modelling, pp. 51–57.

Polve, M., Maury, R.C., Jego, S., Bellon, H., Margoum, A., Yumul, G.P., Payot, B.D., Tamayo, R.A., Cotten, J., 2007. Temporal geochemical evolution of neogene magmatism in the Baguio gold-copper mining district (Northern Luzon, Philippines). Resour. Geol. 57 (2), 197–218.

Roedder, E., Bodnar, R.J., 1980. Geologic pressure determinations from fluid inclusion studies. Ann. Rev. Earth Planetary Sci. 8 (1), 263–301.

Ruelo. H. Jr., Angeles, C., 2017, Diatreme Breccias: Occurrences in Gold ±. Base Metal Epithermal and Porphyry Deposits in the Philippines [abs]: Rushurgent Working Group, Hunt for Ore Deposits: Challenges and Opportunities for Environmental Sustainability, Baguio City, Philippines, 2017, Abstract Volume and Program, p. 13.

Sawkins, F.J., O'Neil, J.R., Thompson, J.M., 1979. Fluid inclusion and geochemical studies of vein gold deposits, Baguio district, Philippines. Econ. Geol. 74, 1420–1434.

Schwarz-Schampera, U., 2014, Antimony. in Gunn, G., ed., Critical Metals Handbook: West Sussex, John Wiley & Sons, Ltd, p. 70-98.

Shimizu, T., 2017. Sulfur isotopic ratios and mode of occurrence of stibnite at the Hishikari epithermal Au-Ag deposit. Japan: Bull. Geol. Survey Japan 68 (3), 111–117.

Sillitoe, R.H., Bonham, H.F., 1984. Volcanic landforms and ore deposits. Econ. Geol. 79, 1286–1298.

Sillitoe, R.H., Hedenquist, J.W., 2003. Linkages between Volcanotectonic Settings, Ore-Fluid Compositions, and Epithermal Precious Metal Deposits. Soc. Econ. Geol. Special Publications 315–343.

Simmons, S.F., 1995. Magmatic contributions to low-sulfidation epithermal deposits: Magmas, fluids and ore deposits. Mineral. Soc. Canada Short Course 23, 455–477.

Spycher, N.F., Reed, M.H., 1989. Evolution of a Broadlands-type epithermal ore fluid along alternative PT paths; implications for the transport and deposition of base, precious, and volatile metals. Econ. Geol. 84, 328–359.

Sweet, G., 2012. Magmatic evolution and alteration geochemistry of the Black Mountain Southeast porphyry copper-gold deposit, Baguio mineral district Luzon, Philippines (Doctoral dissertation).

Takahashi, R., Matsueda, H., Okrugin, V.M., Ono, S., 2007. Epithermal Gold-Silver Mineralization of the Asachinskoe Deposit in South Kamchatka, Russia. Resour. Geol. 57 (4), 354–373.

Tămaș, Călin, Milési, J., 2002. Hydrovolcanic Breccia Pipe Structures-General Features and Genetic Criteria. I. Phreatomagmatic Breccias: Studia Universitatis Babeș-Bolyai (UBB). Geologia 47 (1), 127–147.

United Nations Development Programme (UNDP), 1987. Geology and mineralization in the Baguio area, northern Luzon. United Nations Development Programme, Bureau of Mines and Geosciences, Department of Environment and Natural Resources, Technical Report No. 5, 82 p..

Wallier, S., Rey, R., Kouzmanov, K., Pettke, T., Heinrich, C.A., Leary, S., O'Connor, G., Tamas, C.G., Vennemann, T., Ullrich, T., 2006. Magmatic Fluids in the Breccia-Hosted Epithermal Au-Ag Deposit of Rosia Montana, Romania. Econ. Geol. 101 (5), 923–954.

Waters, P.J., Cooke, D.R., Gonzales, R.I., Phillips, D., 2011. Porphyry and epithermal deposits and $^{40}Ar/^{39}Ar$ geochronology of the Baguio district, Philippines. Econ. Geol. 106 (8), 1335–1363.

Wolfe, J.A., 1986. Breccias related to explosive volcanism. J. Southeast Asian Earth Sci. 1 (2), 63–79.

Yanagisawa, F., Sakai, H., Sakai, H., 1983. Thermal decomposition of barium sulfate-vanadium pentoxide-silica glass mixtures for preparation of sulfur dioxide in sulfur isotope ratio measurements. Anal. Chem. 55 (6), 985–987.

Yumul Jr, G.P., Dimalanta, C.B., Tam III, T.A., Ramos, E.G.L., 2008. Baguio Mineral District: An oceanic arc witness to the geological evolution of northern Luzon, Philippines. Island Arc 17, 432–442.